Available online at www.sciencedirect.com
ScienceDirect
Trans. Nonferrous Met. Soc. China 27(2017) 250−257
Transactions of Nonferrous Metals Society of China
www.tnmsc.cn

Effect of flame rectification on corrosion property of Al−Zn−Mg alloy

Shuai LI, Dan GUO, Hong-gang DONG

School of Materials Science and Engineering, Dalian University of Technology, Dalian 116024, China

Received 5 December 2015; accepted 1 September 2016

Abstract: The corrosion resistance of Al−Zn−Mg alloy subjected to different times in flame rectification was investigated based on the exfoliation corrosion test. The results indicate that the flame rectification deteriorates the exfoliation corrosion resistance of Al−Zn−Mg alloy. The corrosion resistance of Al−Zn−Mg alloy is ranked in the following order: base metal>two times>three times>one time of flame rectification. The exfoliation corrosion behavior was discussed based on the transformation of precipitates at grain boundaries and matrix. With increasing the number of times in flame rectification, the precipitate-free zones disappeared and the precipitates experienced dissolution and re-precipitation. The sample was seriously corroded after one time of flame rectification, because the precipitates at grain boundaries are more continuous than those in other samples.

Key words: Al−Zn−Mg alloy; flame rectification; exfoliation corrosion; re-precipitation

1 Introduction

Al−Zn−Mg alloys have been widely used in structural components due to their high specific strength and good weldability. Metal inert-gas (MIG) arc welding is often used to join Al−Zn−Mg alloys with Al−Mg filler ER5356 in structure components. However, aluminum alloy has high thermal conductivity and thermal expansion coefficient, which results in welding distortion easily. Welding distortion has negative effects on the accuracy of assembly, external appearance, and strengths like tensile strength and fatigue strength, etc., of the welded structures [1,2]. In many cases, additional costs and schedule delays are incurred from correcting welding distortion [3]. Therefore, it is very important to control welding distortion of large welded structures during assembly process. Basically, there are two methods for rectifying welding distortion after welding, namely mechanical rectification and flame rectification [4]. Mechanical rectification is capable of rectifying deformation for small parts, while flame rectification is usually used for large parts such as blocks and subassemblies. Flame rectification is to rectify metal plate by inflation resulted from local heating. Since metallic materials expand when heated and contract when cooled, the metal plate will generate contractive plastic deformation because the swell is hampered by the surrounding relatively cold areas. The new compressive plastic distortions counteract the previous distortions with temperature falling after heating stops [4]. In this way, the precious distortion is counteracted. The flame rectification process after welding has been widely used in actual productive process owing to low cost and easy operation [5−8]. However, flame rectification often affects the corrosion resistance of structure workpieces.

A number of investigations have been carried out to improve the corrosion resistance of aluminum alloys. It has been found that heat treatment can significantly reduce the susceptibility of Al−Zn−Mg alloys [9−11]. Recently, it has been reported that the corrosion resistance of Al−Zn−Mg−Cu alloys could be improved by high-temperature pre-precipitation heat treatment [12,13]. Some researchers also reported that quenching is another important factor that has great impact on corrosion resistance, the results show that decrease of quenching rate often leads to lower exfoliation corrosion resistance [14−16].

Among various corrosion types (pitting corrosion, intergranular corrosion, stress corrosion cracking), exfoliation corrosion (EXCO) as a special form of intergranular corrosion is particularly relevant to the larger aspect ratio of grains in aluminum alloy plates and environment exposure where potential trapping and

Foundation item: Projects (51374048, 50904012) supported by the National Natural Science Foundation of China
Corresponding author: Hong-gang DONG; Tel: +86-411-84706283; Fax: +86-411-84709284; E-mail: donghg@dlut.edu.cn
DOI: 10.1016/S1003-6326(17)60029-3

concentration of water, such as riveted areas, can occur [17,18]. The volume of corrosion products at grain boundaries is larger than that of corroded metals, which leads to internal stress at grain boundaries, followed by grain lift-up that results in formation of blisters on the surface [19,20]. EXCO has been reported to significantly deteriorate the fatigue life of aluminum alloys [21,22]. The EXCO is controlled by intergranular corrosion mainly from two ways: the very anisotropic fibrous grain structure and the precipitate in the electrolyte of corrosion products, which help lift-up the uncorroded grains [20,23]. Many literatures focused on different aging treatments, such as peak aging (T6), over-aging (T7x), retrogression and reaging (RRA) treatments of aluminum alloys and few papers reported T5 condition in recent decades. The T5 condition is defined as a status of aluminum alloy which is cooled in high-temperature molding process and then artificially aged. In recent years, the extrusion profiles of Al−Zn−Mg alloys in T5 condition have been widely used in rail transit industry. In this work, the Al−Zn−Mg alloys are supplied in T5 condition, and the aim is to understand the effect of flame rectification on the corrosion susceptibility of Al−Zn−Mg alloys based on exfoliation corrosion test and microstructure characterization by TEM, and to find out the mechanism leading to the decrease of corrosion resistance and then improve the flame rectification effect on Al−Zn−Mg alloys.

2 Experimental

The base material used in this work was 10 mm-thick extruded Al−Zn−Mg alloy plate in T5 condition, as shown in Fig. 1. The chemical composition and some basic properties of this alloy are listed in Table 1 and Table 2, respectively. The samples were heated using oxygen−propane flame to 350 °C (±10 °C) for different times, and the details are listed in Table 3. The temperature of heated samples was measured by a Tempilstic temperature pen (TS0350) during flame rectification, and the torch moved at a constant speed around the heated area to achieve uniform distribution of temperature. After flame rectification, the samples were quenched by water immediately.

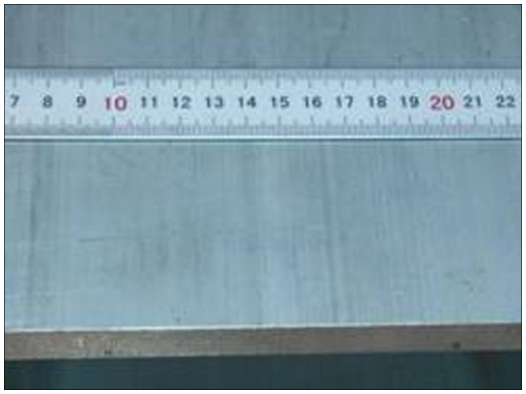

Fig. 1 Profile of as-supplied Al−Zn−Mg alloy

Table 1 Chemical composition of Al−Zn−Mg alloy (mass fraction, %)

Zn	Mg	Mn	Cr	Zr	Fe
4.480	1.547	0.294	0.232	0.180	0.125

Cu	Ti	Si	V	Al
0.113	0.054	0.050	0.014	Bal.

Table 2 Mechanical properties of Al−Zn−Mg alloy

Tensile strength/ MPa	Yield strength/ MPa	Elongation/ %	Hardness (HV)	Conductivity/ %IACS
360	295	20.6	104.3	36.5

Table 3 Flame rectification parameters for Al−Zn−Mg alloy

Sample	Temperature/ °C	Corrosion times	Corrosion time/s
FR0	−	−	−
FR1	350	1	120
FR2	350	2	120
FR3	350	3	120

According to the Chinese National Standard GB/T 22639−2008, the samples in dimensions of 100 mm × 35 mm × 10 mm were prepared for exfoliation corrosion test [24]. The exfoliation corrosion solution was prepared by following steps: Dissolve 234 g of reagent grade NaCl, 50 g of KNO_3 in distilled water, and add 6.3 mL of concentrated HNO_3 (70%) then dilute to 1 L. So, the solution contains 4.0 mol NaCl, 0.5 mol KNO_3 and 0.1 mol HNO_3. The specimens were immersed in the corrosion solution for 48 h with the temperature maintained at (25±2) °C. The exposed area is 35 cm^2, and the ratio of solution volume to metal surface is 35 mL/cm^2. The surface morphologies after immersion test were examined by scanning electron microscopy (SEM). Moreover, the corrosion resistance was evaluated by a confocal laser scanning microscope (CLSM). In order to quantitatively analyze the corrosion susceptibility of the specimens, the average height difference was measured based on the CLSM pictures. To obtain the height difference along *X*-axis, the cross sections paralleling to *X*-axis were obtained (the cross sections were equidistant), then the height difference was acquired through the height variation curves, as shown in Fig. 2. Ten different areas with the sizes of 2560 μm × 2560 μm of the specimens were measured, then the average of height difference was calculated. Similarly, the height difference along *Y*-axis was obtained.

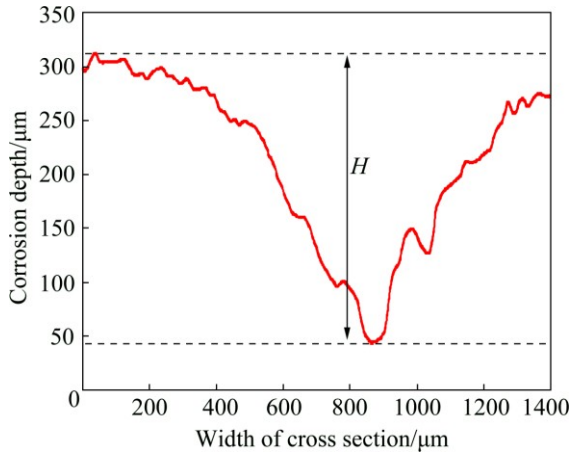

Fig. 2 Height variation curve of cross section

Samples in the dimensions 10 mm × 10 mm × 0.5 mm were sectioned from the plates for TEM examination. After grinding and polishing, the samples were made into 100 μm-thick foils followed by double electro-polishing in a solution of 25% HNO_3 + 75% CH_3OH (volume fraction) with voltage of 20 V at −25 °C. TEM test was carried out at 200 kV on a Tecnai G^2 20S-Twin equipment.

3 Results and discussion

3.1 Optical microstructure

Figure 3 reveals the optical micrographs of the samples suffered in flame rectification at 350 °C for different times. The fibrous grain structure is quite typical in extruded high strength Al−Zn−Mg alloys, and this provides condition for exfoliation corrosion [17,19,25]. The microstructures of Al−Zn−Mg alloy are nearly unchanged after different times in flame rectification, which is likely associated with the recrystallization temperature of Al−Zn−Mg alloy (~460 °C) and heating parameters (Table 3). In addition, the modification of precipitates in Al−Zn−Mg alloy, such as GP zones, η' and η phases, could not be observed through optical microscope. The black particles in Fig. 3 were identified to be α-AlFeMnSi phases [26], which often formed in Al−Zn−Mg alloy. Generally, these particles have little effect on exfoliation corrosion and thus will not be discussed hereafter.

3.2 Exfoliation corrosion test

After EXCO test, the corrosion susceptibility was evaluated in different testing equipment. Figure 4 shows the corrosion morphology of each sample still in wet state after finishing the test. It can be seen that the sample FR0 just lost metallic luster and no significant corrosion features appeared. However, the corrosion susceptibility of the specimens suffering different times in flame rectification increased compared with the base metal, as displayed in Figs. 4(b)−(d). The sample FR1 is the most seriously corroded in EXCO test judging from the macroscopic pictures of the corroded samples, especially in area *A* in Fig. 4(b). In Fig. 4(c), the sample FR2 reveals better exfoliation corrosion resistance than that of sample FR1 and uncorroded areas could be clearly seen on sample FR2. In Fig. 4(d), an uncorroded

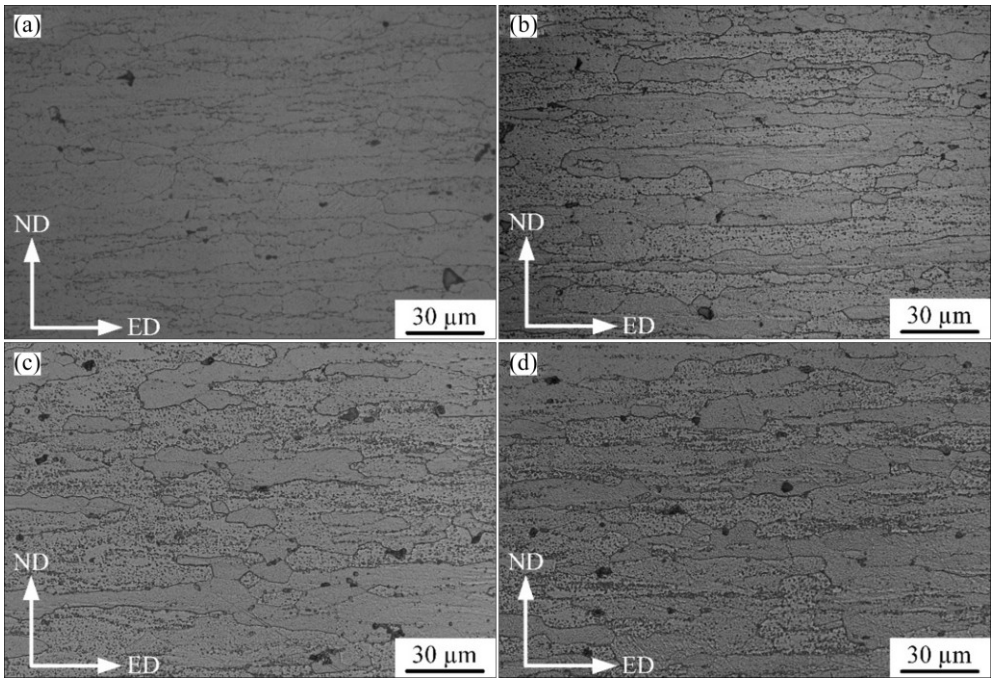

Fig. 3 Optical micrographs of base metal (a) and samples after one time (b), two times (c), and three times (d) of flame rectification at 350 °C for Al−Zn−Mg alloy (ED: extruding direction; ND: normal direction)

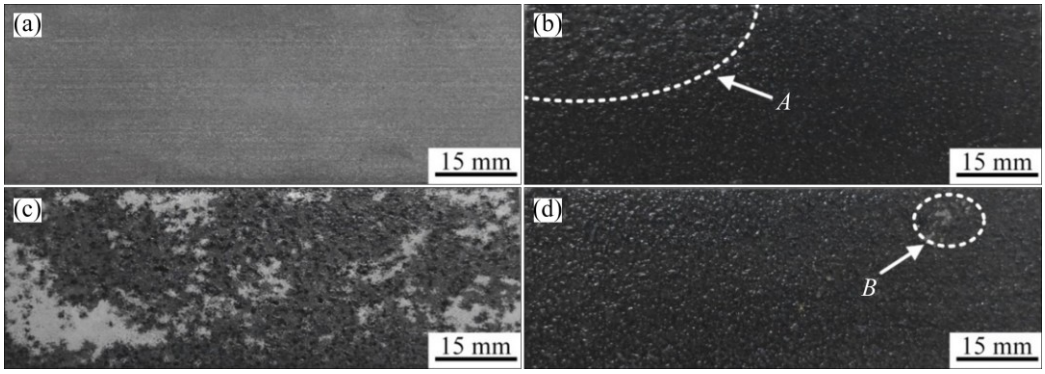

Fig. 4 Corrosion morphology of corroded samples still in wet state of base metal (a), and samples after one time (b), two times (c), and three times (d) of flame rectification at 350 °C after exfoliation test for 48 h

surface *B* exists and the corrosion sensitivity of sample FR3 is between that of samples FR1 and FR2.

Figure 5 presents the SEM images of samples after EXCO test in dry state. The corroded surface of sample FR0 is full of cracks without obvious exfoliation corrosion characteristics, as shown in Fig. 5(a). However, the morphologies of the samples in dry state varies significantly. Corrosion penetrates into sample FR1 in Fig. 5(b), which is much heavier than that of sample FR2 in Fig. 5(c) and sample FR3 in Fig. 5(d), owing to internal stress at grain boundaries.

In order to obtain more details about the corrosion resistance of heated samples, 3D optical micrographs of the specimens after different times in flame rectification were obtained after immersion in EXCO solution for 48 h, as revealed in Fig. 6. It can be clearly seen that the samples show different morphologies and the corrosion susceptibility increases after flame rectification. As seen in Fig. 6(a), the surface of specimen FR0 is flat, and there are no evident corrosion characteristics. However, after flame rectification, the specimens display typical corrosion characteristics just like hilly terrain morphology. The fluctuation of corroded surface is observed in sample FR1, and the maximum height difference is 382.4 μm as shown in Fig. 6(b). The height difference of corroded surface is smaller for samples FR2 and FR3 than that of sample FR1, but still much higher than that of sample FR0 (base metal). Visual examination is difficult to detect small height difference of corrosion, because its evaluation of corrosion level is subjective and qualitative. In order to quantitatively analyze the corrosion susceptibility, the height difference of corrosion of Al−Zn−Mg alloy was measured under CLSM according to Standard ASTM G34 [27], as listed in Table 4. The height difference of corroded surface ranks in the following order: FR1>FR3>FR2>FR0.

3.3 Grain boundary

During flame rectification, different microstructural changes are likely to occur, such as recrystallization, grain growth and modification of precipitates. The modification of precipitates involves the dissolution of precipitates, growth or transformation of coherent precipitates to incoherent forms. Figure 7 shows the microstructures at grain boundaries after different times in flame rectification at 350 °C. As shown in Fig. 7(a), the precipitate-free zone (PFZ) in specimen FR0 is narrow (less than 30 nm on each side of the boundary), and the grain boundaries contain discontinuous precipitates, which are beneficial to decrease the corrosion susceptibility [9−11]. In order to clarify category of the precipitate phases, the selected area diffraction patterns (SADPs) of matrix precipitates (MPts) and grain boundary precipitates (GBPs) from sample FR0 were obtained, as shown in Fig. 8. The main strong diffraction spots come from the aluminum alloy matrix. The SADP analysis in matrix indicates that the extra diffraction spots are mainly from the η' and η phases contributing to aluminum alloys strength [28], and the GBPs are identified to be η phases after flame rectification, the precipitate phases change obviously, especially the MPt. The grain boundary precipitates become more continuous compared with base metal, as seen in Fig. 7(b), which is harmful to the corrosion resistance of aluminum alloys [9−11]. In Fig. 7(c), there are almost no precipitate phases in the aluminum alloy matrix and along the grain boundaries. After three times of flame rectification, the grain boundary precipitates appear again, as seen in Fig. 7(d), and some sporadic precipitates form in matrix. The precipitate phases experience dissolution and re-precipitation with increasing the times in flame rectification. The modification of precipitates is associated with the corrosion susceptibility of aluminum alloy [29].

The exfoliation corrosion resistance of Al−Zn−Mg alloy decreases after flame rectification, as shown in Figs. 4−6. The precipitate phases, including the metastable phases GP, η' and stable phase η, dissolve

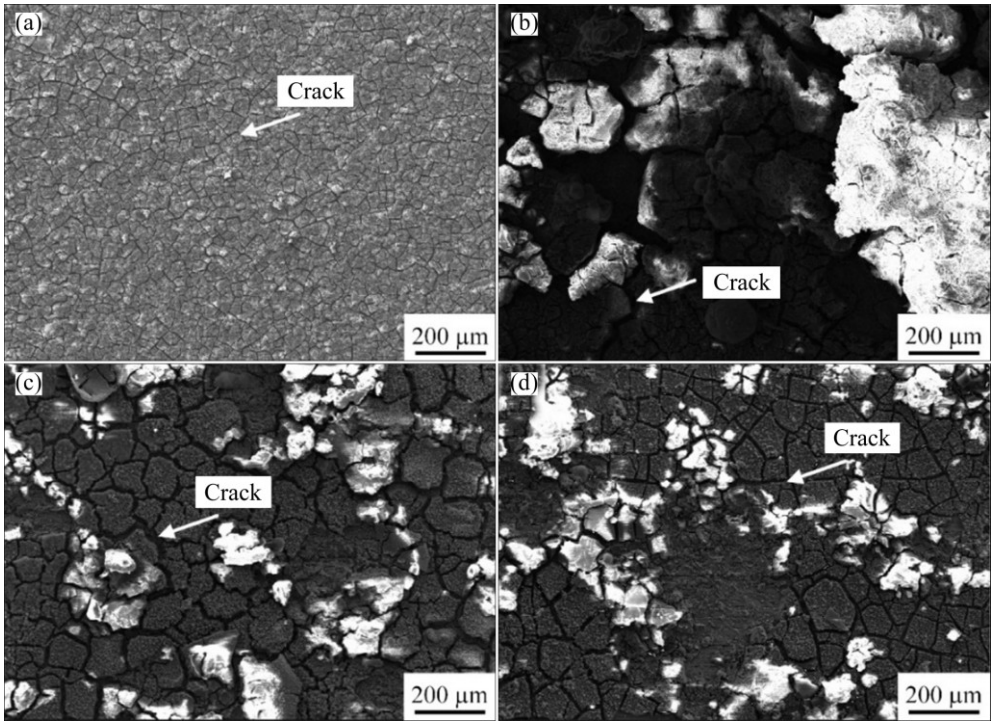

Fig. 5 SEM images of base metal (a), and samples after one time (b), two times (c), and three times (d) of flame rectification at 350 °C after exfoliation corrosion test (in dry state)

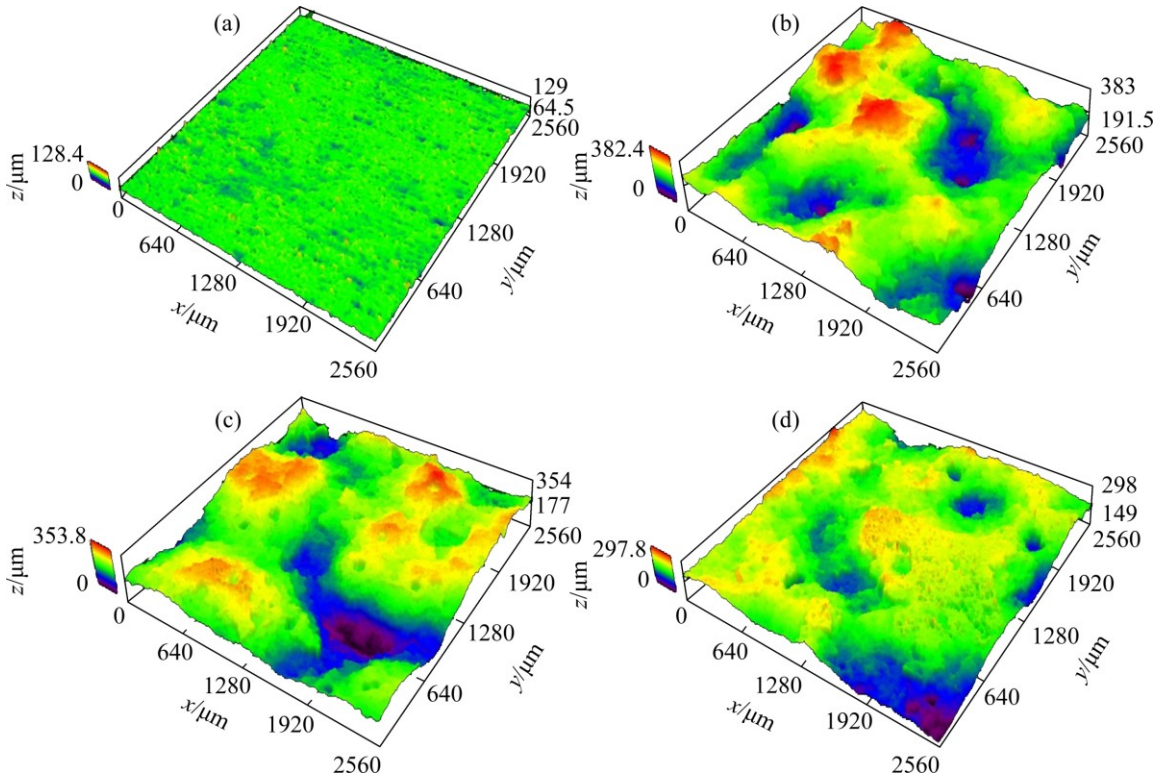

Fig. 6 Three-dimensional optical micrographs without corrosion products of base metal (a), and samples after one time (b), two times (c), and three times (d) of flame rectification at 350 °C after EXCO test

completely at temperature of 340 °C [30]. So, after one time of flame rectification at 350 °C, most of the MPts (η' and η phases) dissolve into the aluminum alloy matrix, and the coarse grain boundary precipitates and a small amount of MPts still exist due to the short dwell time of heating (within 2 min), as shown in Fig. 7(b).

Table 4 Height difference of corroded surface of all samples after EXCO test

Sample	Height difference of corroded surface/μm	Cross section
FR0	<15	*X*-axis
	<20	*Y*-axis
FR1	245	*X*-axis
	232	*Y*-axis
FR2	95	*X*-axis
	100	*Y*-axis
FR3	175	*X*-axis
	163	*Y*-axis

With increasing the number of times in flame rectification, the precipitate phases in Fig. 7(c) continue to dissolve and form the super-saturated solid solution. For the formation of super-saturated solid solution in aluminum alloy, the third flame rectification can be seen with pre-precipitation heat treatment. It is well-known that Al−Zn−Mg alloys tend to precipitate at grain boundaries [13]. The grain precipitation is limited, and only a few stable phases preferentially precipitate at the grain boundaries, because the dwell time of heating is short, and the driving force for precipitation is too small to reach the nucleation energy.

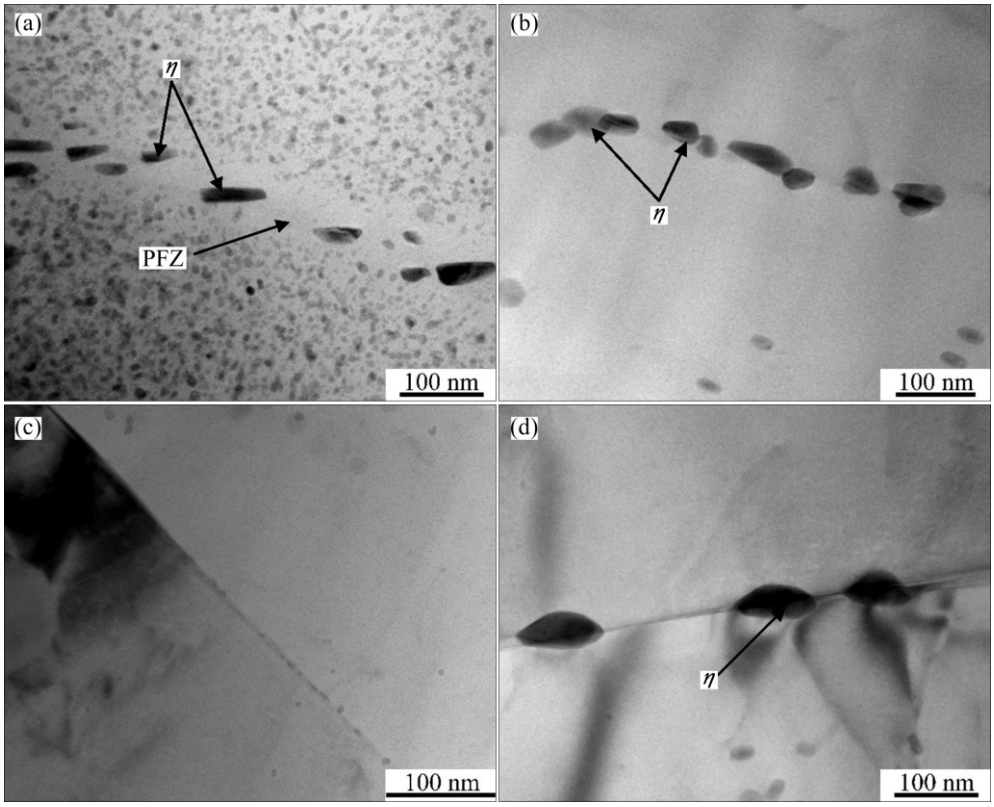

Fig. 7 Microstructures of grain boundaries in base metal (a), and samples after one time (b), two times (c), and three times (d) of flame rectification at 350 °C

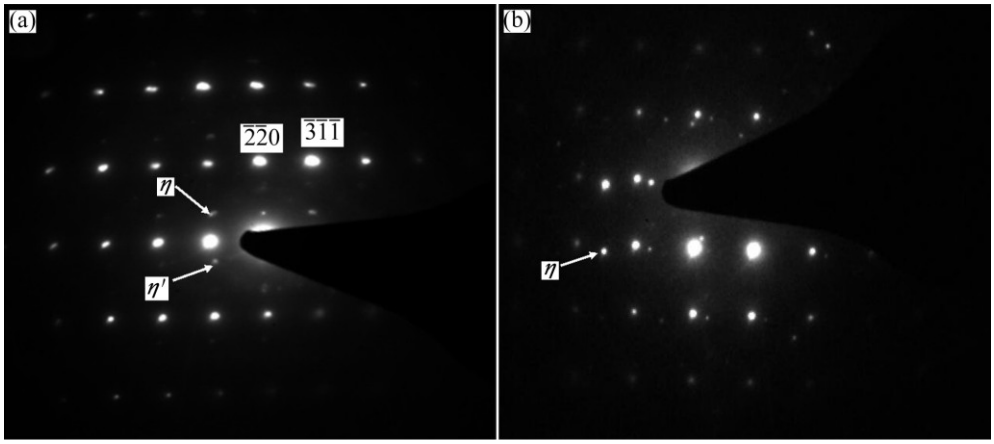

Fig. 8 SAD patterns of matrix precipitates (a) and grain boundary precipitates (b) in base metal

According to the anodic dissolution mechanism, the driving force for corrosion of Al−Zn−Mg alloy is the potential difference between the grain boundary precipitates η ($MgZn_2$) and the matrix [14,20]. The η phases always act as the anode, the PFZ and matrix act as the cathode. The precipitates at grain boundaries in sample FR1 are more continuous than those of the other samples, therefore, the sample FR1 is most seriously corroded in this test [14,19,31]. For specimen FR2, nearly all the precipitates dissolved into the matrix, and the potential difference between the grain boundary and matrix decreases, reducing the degree of corrosion. With increasing the number of times in flame rectification, the η phases precipitate again at the grain boundaries, so, the potential difference increases and then results in the increase of degree of corrosion.

4 Conclusions

1) The flame rectification deteriorates the exfoliation corrosion resistance of Al−Zn−Mg alloy. The exfoliation corrosion resistance ranks in the following order: base metal>two times>three times>one time.

2) After one time of flame rectification, the grain boundary precipitates become more continuous, which provide more continuous propagation path of exfoliation corrosion and result in the most serious corrosion. After two times of flame rectification, the precipitates in the alloy continue to dissolve and super-saturated solid solution forms, and then the potential difference between the grain boundary and matrix decreases, reducing the degree of corrosion. The third flame rectification can be seen with pre-precipitation heat treatment for Al−Zn−Mg alloy, and a few stable phases preferentially precipitate at the grain boundaries, which increases the potential difference and the degree of corrosion.

3) After different times in flame rectification, the precipitate-free zones disappear and the precipitates experience dissolution and re-precipitation.

References

[1] DENG D, MURAKAWA H, LIANG W. Numerical simulation of welding distortion in large structures [J]. Computer Methods in Applied Mechanics & Engineering, 2007, 196(s45−48): 4613−4627.

[2] JUNG H, TSAI C L. Plasticity-based distortion analysis for fillet welded thin-plate T-joints [J]. Welding Journal, 2004, 83: 177−187.

[3] DENG D, MURAKAWA H. Prediction of welding distortion and residual stress in a thin plate butt-welded joint [J]. Computer Material Science, 2008, 43(2): 353−365.

[4] ZHANG Zhi-ying, JIANG Zhi-bin, YU Cheng-quan. Automated flame rectification process planning system in shipbuilding based on artificial intelligence [J]. International Journal of Advanced Manufacturing Technology, 2006, 30(11): 1119−1125.

[5] LIU Chun-ning, WANG Lu-zhao, HU Wen-hao, YU Jin-peng. Numerical simulation method of welding and multi-adjusting for EN-AW 6082 aluminum alloy [J]. Welding Technology, 2012, 41: 11−16. (in Chinese)

[6] XIONG Zhi-liang, Effect mechanism of heat-straightening temperature on microstructure and properties of aluminum alloy joint in high-speed trains [D]. Harbin, Harbin Institute of Technology, 2014. (in Chinese)

[7] LACALLE R, ÁLVAREZ J A, FERREÑO D, PORTILLA J, RUIZ E, ARROYO B, GUTIÉRREZ-SOLANA F. Influence of the flame straightening process on microstructural, mechanical and fracture properties of S235 JR, S460 ML and S690 QL structural steels [J]. Experimental Mechanics, 2013, 53(6): 893−909.

[8] JIANG Lan, WANG Yan-jin, LIU Ai-jun, WEI Xu-jun. Effect of flame straightening on microstructures and properties of welded Joint of aluminium alloy for high-speed train [J]. Transactions of Materials and Heat Treatment, 2003, 24(4): 59−61. (in Chinese)

[9] PENG Guo-sheng, CHEN Kang-hua, CHEN Song-yi, FANG Hua-chan. Influence of dual retrogression and re-aging temper on microstructure, strength and exfoliation corrosion behavior of Al−Zn−Mg−Cu alloy [J]. Transactions of Nonferrous Metals Society of China, 2012, 22(22): 803−809.

[10] ROMETSCH P A, ZHANG Y, KNIGHT S. Heat treatment of 7xxx series aluminium alloys-some recent developments [J]. Transactions of Nonferrous Metals Society of China, 2014, 24(7): 2003−2017.

[11] ZHOU Kun, WANG Bin, ZHAO Yong, LIU Jie. Corrosion and electrochemical behaviors of 7A09 Al−Zn−Mg−Cu alloy in chloride aqueous solution [J]. Transactions of Nonferrous Metals Society of China, 2015(8), 25: 2509−2515.

[12] CHEN Kang-hua, HUANG Lan-ping. Strengthening-toughening of 7xxx series high strength aluminum alloys by heat treatment [J]. Transactions of Nonferrous Metals Society of China, 2003, 13(3): 484−490.

[13] HUANG Lan-ping, CHEN Kang-hua, LI Song. Influence of grain-boundary pre-precipitation and corrosion characteristics of inter-granular phases on corrosion behaviors of an Al−Zn−Mg−Cu alloy [J]. Materials Science & Engineering B, 2012, 177(11): 862−868.

[14] SONG Feng-xuan, ZHANG Xin-ming, LIU Sheng-dan, QI Tan, LI Dong-feng. The effect of quench rate and overageing temper on the corrosion behaviour of AA7050 [J]. Corrosion Science, 2014, 78(8): 276−286.

[15] LIU Sheng-dan, LI Cheng-bo, DENG Yun-lai, ZHANG Xin-ming. Influence of grain structure on quench sensitivity relative to localized corrosion of high strength aluminum alloy [J]. Materials Chemistry & Physics, 2015, 167: 320−329.

[16] CHEN Song-yi, CHEN Kang-hua, PENG Guo-sheng. Effect of quenching rate on microstructure and stress corrosion cracking of 7085 aluminum alloy [J]. Transactions of Nonferrous Metals Society of China, 2012, 22(1): 47−52.

[17] ROBINSON M J, JACKSON N C. The influence of grain structure and intergranular corrosion rate on exfoliation and stress corrosion cracking of high strength Al−Cu−Mg alloys [J]. Corrosion Science, 1999, 41(5): 1013−1028.

[18] KNIGHT S P, BIRBILIS N, MUDDLE B C. Correlations between intergranular stress corrosion cracking, grain-boundary microchemistry, and grain-boundary electrochemistry for Al−Zn−Mg−Cu alloys [J]. Corrosion Science, 2010, 52(12): 4073−4080.

[19] SONG Feng-xuan, ZHANG Xin-ming, LIU Sheng-dan, TAN Qi, LI Dong-feng. Exfoliation corrosion behavior of 7050-T6 aluminum alloy treated with various quench transfer time [J]. Transactions of Nonferrous Metals Society of China, 2014, 24(7): 2258−2265.

[20] MARLAUD T, MALKI B, HENON C. Relationship between alloy composition, microstructure and exfoliation corrosion in Al−Zn−Mg−Cu alloys [J]. Corrosion Science, 2011, 53(10):

3139−3149.
[21] LIAO M, RENAUD G, BELLINGER N C. Fatigue modeling for aircraft structures containing natural exfoliation corrosion [J]. International Journal of Fatigue, 2007, 29(4): 677−686.
[22] BURNS J T, KIM S, GANGLOFF R P. Effect of corrosion severity on fatigue evolution in Al−Zn−Mg−Cu [J]. Corrosion Science, 2010, 52(2): 498−508.
[23] LI J F, JIA Z Q, LI C X, BIRBILIS N, CAI C. Exfoliation corrosion of 7150 Al alloy with various tempers and its electrochemical impedance spectroscopy in EXCO solution [J]. Materials & Corrosion, 2009, 60(6): 407−414.
[24] GB/T 22639—2008. Standard test method for exfoliation corrosion susceptibility in 2xxx and 7xxx series aluminum alloys [S]. 2008.
[25] FAN Xi-gang, JIANG Da-ming, ZHONG Li, WANG Tao, REN Shi-yu. Influence of microstructure on the crack propagation and corrosion resistance of Al−Zn−Mg−Cu alloy 7150 [J]. Materials Characterization, 2007, 58(1): 24−28.
[26] HODGSON P, PARKER B A. The composition of insoluble intermetallic phases in aluminium alloy 6010 [J]. Journal of Materials Science, 1981, 16(5): 1343−1348.
[27] ASTM Standard G34-01. Standard test method for exfoliation corrosion susceptibility in 2xxx and 7 xxx series aluminum alloys (EXCO Test) [S]. 2013.
[28] SHA G, CEREZO A. Early-stage precipitation in Al−Zn−Mg−Cu alloy (7050) [J]. Acta Materialia, 2004, 52(15): 4503−4516.
[29] MA T, OUDEN G D. Softening behaviour of Al−Zn−Mg alloys due to welding [J]. Materials Science & Engineering A, 1999, 266(266): 198−204.
[30] FANG Lei, ZHAO Xin-qi, CHEN Jiang-hua, LIU Ji-zi, YANG Xiu-bo, LIU Ping, MING Wen-quan, WU Cui-lan. Study of the precipitation behaviors in a triple-step-aged Al−Zn−Mg alloy [J]. Journal of Chinese Electron Microscopy Society, 2012, 31(3): 202−210. (in Chinese)
[31] LIU S D, CHEN B, LI C B, DAI Y, DENG Y L, ZHANG X M. Mechanism of low exfoliation corrosion resistance due to slow quenching in high strength aluminium alloy [J]. Corrosion Science, 2015, 91: 203−212.

火焰矫正对 Al−Zn−Mg 铝合金腐蚀性能的影响

李 帅，郭 丹，董红刚

大连理工大学 材料科学与工程学院，大连 116024

摘 要：基于剥落腐蚀试验，研究了火焰矫正次数对 Al−Zn−Mg 铝合金抗腐蚀性能的影响。结果表明，火焰矫正会导致 Al−Zn−Mg 铝合金抗腐蚀性能降低，其抗腐蚀性能顺序为：母材>2 次热矫正>3 次热矫正>1 次热矫正。Al−Zn−Mg 铝合金剥落腐蚀性能变化主要与晶界析出相以及基体析出相的转变有关。随着火焰矫正次数的增加，无沉淀析出带消失，晶界析出相经历了回溶和再析出过程。经 1 次火焰矫正后，Al−Zn−Mg 铝合金的晶界析出相更加连续，因此抗腐蚀性能最差。

关键词：Al−Zn−Mg 铝合金；火焰矫正；剥落腐蚀；再析出

(Edited by Xiang-qun LI)